Check for updates

AGU ADVANCING EARTH AND SPACE SCIENCES

JGR Atmospheres

RESEARCH ARTICLE
10.1029/2024JD042412

Recent Lower Stratospheric Ozone Trends in CCMI-2022 Models: Role of Natural Variability and Transport

Samuel Benito-Barca[1,2], Marta Abalos[1], Natalia Calvo[1], Hella Garny[3], Thomas Birner[4], Nathan Luke Abraham[5,6], Hideharu Akiyoshi[7], Fraser Dennison[8,9], Patrick Jöckel[3], Bèatrice Josse[10], James Keeble[11], Doug Kinnison[12], Marion Marchand[13], Olaf Morgenstern[14,15,16], David Plummer[17], Eugene Rozanov[18], Sarah Strode[19,20], Timofei Sukhodolov[18], Shingo Watanabe[21], and Yousuke Yamashita[7]

[1]Departamento de Física de la Tierra y Astrofísica, Universidad Complutense de Madrid, Madrid, Spain, [2]Instituto de Geociencias (IGEO), Consejo Superior de Investigaciones Científicas–Universidad Complutense de Madrid (CSIC–UCM), Madrid, Spain, [3]Institut für Physik der Atmosphäre, Deutsches Zentrum für Luft- und Raumfahrt (DLR), Oberpfaffenhofen, Germany, [4]Meteorologisches Institut, Ludwig-Maximilians-Universität München, Munich, Germany, [5]National Centre for Atmospheric Science, University of Cambridge, Cambridge, UK, [6]Yusuf Hamied Department of Chemistry, University of Cambridge, Cambridge, UK, [7]Earth System Division, National Institute for Environmental Studies, Ibaraki, Japan, [8]CSIRO Environment, Melbourne, VIC, Australia, [9]School of Geography, Earth and Atmospheric Sciences, University of Melbourne, Melbourne, VIC, Australia, [10]CNRM, Université de Toulouse, Météo-France, CNRS, Toulouse, France, [11]Lancaster Environment Centre, Lancaster University, Lancaster, UK, [12]National Center for Atmospheric Research, Boulder, CO, USA, [13]LATMOS, Institut Pierre-Simon Laplace, Sorbonne Université/CNRS/UVSQ, Paris, France, [14]National Institute of Water and Atmospheric Research, Wellington, New Zealand, [15]School of Physical and Chemical Sciences, Canterbury University, Christchurch, New Zealand, [16]Now at: Deutscher Wetterdienst, Offenbach, Germany, [17]Climate Research Division, Environment and Climate Change Canada, Montreal, QC, Canada, [18]Physikalisch-Meteorologisches Observatorium Davos/World Radiation Center, Davos, Switzerland, [19]Atmospheric Chemistry and Dynamics Laboratory, NASA Goddard Space Flight Center (GSFC), Greenbelt, MD, USA, [20]GESTAR II, Morgan State University, Baltimore, MD, USA, [21]Research Center of Global Change (RIGC) and WPI-AIMEC, Japan Agency for Marine-Earth Science and Technology (JAMSTEC), Yokohama, Japan

Key Points:

- Chemistry-climate models with observed sea surface temperatures can capture the recent decline in mid-latitude lower stratospheric ozone
- Trends over 1998–2018 are due to internal variability and not a linear response to the main climate variability modes or external forcings
- Large intermodel differences are due to different representations of ozone transport processes and their internal variability

Supporting Information:

Supporting Information may be found in the online version of this article.

Correspondence to:

S. Benito-Barca,
samubeni@ucm.es

Citation:

Benito-Barca, S., Abalos, M., Calvo, N., Garny, H., Birner, T., Abraham, N. L., et al. (2025). Recent lower stratospheric ozone trends in CCMI-2022 models: Role of natural variability and transport. *Journal of Geophysical Research: Atmospheres*, *130*, e2024JD042412. https://doi.org/10.1029/2024JD042412

Received 5 SEP 2024
Accepted 20 APR 2025

Abstract Lower stratospheric ozone between 60°S and 60°N has continued to decline since 1998, despite the reduction of ozone-depleting substances following the Montreal Protocol. Previous studies have shown that, while chemistry-climate models reproduce the negative ozone trend in the tropical lower stratosphere as a response to increased upwelling, they fail to capture the ozone decline in northern midlatitudes. This study revisits recent lower stratospheric ozone trends over the period 1998–2018 using two types of simulations from the new Chemistry Climate Model Initiative 2022 (CCMI-2022): REF-D1, with observed sea surface temperatures, and REF-D2, with simulated ocean. The observed negative trend in midlatitudes falls within the range of model trends, especially when considering simulations with observed boundary conditions. There is a large spread in the simulated midlatitudes ozone trends, with some simulations showing positive and others negative trends. A multiple linear regression analysis shows that the spread in the trends is not explained by the different linear response to external forcings (solar cycle, global warming, and ozone-depleting substances) or to the main variability modes (El Niño-Southern Oscillation and the quasi-biennial oscillation) but is instead attributed to internal atmospheric variability. Moreover, the fact that some models show very different trends across members, while other models show similar trends in all members, suggests fundamental differences in the representation of the internal variability of ozone transport across models. Indeed, we report substantial intermodel differences in the ozone-transport connection on interannual timescales and we find that ozone trends are closely coupled to transport trends.

Plain Language Summary Stratospheric ozone is essential for life as it protects from harmful solar ultraviolet radiation. In the late 20th century, the anthropogenic emission of ozone-depleting substances (ODS), especially chlorofluorocarbons (CFCs), significantly reduced the ozone layer, leading to the adoption in 1987 of the Montreal Protocol to regulate CFC production and consumption. However, in some regions, lower stratospheric ozone have continued to decline since 1998. In this work, we revisit ozone trends over 1998–2018 using state-of-the-art chemistry-climate models. We find that chemistry-climate models with observed sea surface temperatures are able to capture the recent decline in midlatitude lower stratospheric ozone, but there are discrepancies between different models. These ozone trends are due to internal variability of the atmosphere rather than a linear response to the main climate variability modes (El Niño-Southern Oscillation or the quasi-biennial oscillation) or to external forcings (solar cycle, global warming, and ODS). We show that stratospheric ozone trends are related to transport trends, and indeed, the differences between models come from differences in the ozone transport and its interannual variability in each model. This highlights the need to better understand atmospheric transport processes in order to improve modeling of past and future ozone trends.

1. Introduction

Stratospheric ozone is a crucial component of the climate system, exerting a key role in the radiative budget and in protecting the Earth from harmful solar ultraviolet (UV) radiation. In the late 20th century, stratospheric ozone was drastically reduced due to anthropogenic emissions of ozone-depleting substances (ODS), especially chlorofluorocarbons (CFC). This problem was tackled by the 1987 Montreal Protocol and subsequent amendments and, as a result, the concentration of ODS in the stratosphere has been declining since the mid-late 1990s (Newman et al., 2007; WMO, 2022). As a consequence, total stratospheric ozone is expected to recover to pre-1980 levels over the 21st century (Chipperfield et al., 2017; Dhomse et al., 2018; Keeble et al., 2021; WMO, 2022).

The recovery of ozone is not only affected by the decline of ODS concentrations but also by the increase of greenhouse gases (GHG). The GHG-induced stratospheric cooling slows down temperature-dependent catalytic ozone loss reactions and thus increases ozone, especially in the upper stratosphere (Brasseur & Hitchman, 1988; Oman et al., 2010). Moreover, increasing anthropogenic GHG emissions accelerates the stratospheric residual circulation (Abalos et al., 2021; Butchart, 2014), enhancing ozone transport from the tropical lower stratosphere to higher latitudes. In addition to the dependence on ODS and GHGs, recent studies have reported a non-negligible future contribution of very short-lived halogens substances (VSLS) in the tropical lower stratosphere (Villamayor et al., 2023).

In recent years, motivated by the turnaround of the ODS concentration in the mid-90s, several studies have looked for signs of recovery of the ozone layer. Indeed, total column ozone (TCO) recovery over Antarctica has already been detected during austral spring (Pazmiño et al., 2018; Solomon et al., 2016) and, very recently, Weber et al. (2022) showed that the near-global (60°N–60°S) TCO trend is on the verge of a statistically significant increase. In contrast, TCO trends in northern midlatitudes and tropics are not significant despite the increase of ozone in the troposphere (Ball et al., 2018; Gaudel et al., 2020; Zhang et al., 2021; Ziemke et al., 2019) and upper stratosphere (Ball et al., 2020; Dietmüller et al., 2021; Godin-Beekmann et al., 2022; Petropavlovskikh et al., 2019; Steinbrecht et al., 2017). These increases have to be offset by changes in the lower and the middle stratosphere, and indeed, there is evidence that ozone in the lower stratosphere has continued to decline since 1998, although the statistical significance of these trends depends on the methodology and data source used in each study (Ball et al., 2018, 2019, 2020; Bognar et al., 2022; Chipperfield et al., 2018; Godin-Beekmann et al., 2022; Orbe et al., 2020; Wargan et al., 2018; Zeng et al., 2024). In the tropics, negative ozone trends in the lower stratosphere are caused by enhanced tropical upwelling due to climate change, which raises more ozone-poor air from the tropopause region where the ozone concentration is more than an order of magnitude lower (Dietmüller et al., 2021; WMO, 2022), and the role of VSLS (Villamayor et al., 2023). However, negative ozone trends at midlatitudes are not so easy to understand. In this region, vertical advection by the residual circulation tends to increase the ozone concentration, while horizontal mixing has the opposite effect (Abalos et al., 2013). The expected enhanced downwelling, balancing the enhanced upwelling in the tropics, should lead to an increase in ozone in the midlatitudes, which is not found in the observations.

Previous studies are often contradictory about the reasons for the observed negative ozone trends. By using a nine-member ensemble of free-running model simulations, Stone et al. (2018) indicated that dynamical variability dominates the ozone changes in this region over 1998–2016. Wargan et al. (2018) suggested, using MERRA-2 reanalysis, that the negative trend in the midlatitude lower stratosphere could be due to increased mixing between the tropics and midlatitudes. This idea was partially supported by Ball et al. (2020), who found that the CCMVal2 models with the highest mixing efficiency were also those simulating negative trends at midlatitude and provided evidence that mixing across subtropics increased in the period 1998–2016. On the other hand, Orbe et al. (2020) found, using the GEOS general circulation model, that the recent ozone changes in the lower stratosphere at northern subtropics and midlatitudes are mainly driven by a poleward expansion of the shallow branch of the residual circulation. Chipperfield et al. (2018), by extending the period by 1 year to 1998–2017, did not find any robust trend and concluded that the previously reported trends in lower stratospheric (LS) ozone were the result of large natural variability rather than long-term changes. However, further studies have shown that although natural variability plays an important role in the northern midlatitudes LS ozone trends, the observed negative trend is robust even when changing the end points of the period by a few years (Ball et al., 2019, 2020; Dietmüller et al., 2021; Godin-Beekmann et al., 2022).

Previous studies have applied a multimodel approach to investigate how well chemistry-climate models (CCMs) reproduce the observed trend patterns in the middle latitudes of the lower stratosphere. Ball et al. (2018) showed for the first time the inability of two CCM models run with specified dynamics to reproduce LS ozone trends. Following this, Ball et al. (2020) and Dietmüller et al. (2021), by using CCMVal2 and CCMI-1 simulations, respectively, concluded that these models were not able to reproduce the observed trend pattern in the lower stratosphere. Instead of a decrease, both sets of models simulated an increase in midlatitudes. Both studies discussed different reasons to explain this disagreement, such as the misrepresentation of ozone transport processes in the models, the misrepresentation of ODS and GHG effect on LS ozone, or that natural variability is not well captured in these sets of models. To our knowledge, the actual reasons for the discrepancies in LS ozone trends between models and observations have not been identified to date.

Importantly, the multimodel evaluations of recent ozone trends by Ball et al. (2020) and Dietmüller et al. (2021) only used long-term simulations with sea surface temperatures (SST) simulated by a coupled climate model, as neither CCMVal2 nor CCMI-1 provided simulations with historical boundary conditions covering the observed period up to 2016 or later (CCMVal2 up to 2006 and CCMI-1 up to 2013). This raises the question whether the particular climate variability over the period of interest may have played a role in the observed ozone trends. We therefore take advantage of the latest Chemistry Climate Model Initiative 2022 (CCMI-2022), which provides historical simulations with observed climate variability extending up to 2018, in addition to long-term simulations with modeled ocean. This allows us to revisit recent ozone trends in the new generation of the model and further study the impact of natural climate variability and transport on these trends by comparing simulations with and without observed natural variability.

The remainder of the paper is organized as follows: a brief description of the methodology, observational data set, and model simulations analyzed is presented in Section 2. Section 3.1 provides a detailed assessment of ozone trends in CCMI-2022 models over the period 1998–2018, while Sections 3.2 and 3.3 analyze how ozone trends are affected by natural and forced variability and link them to changes in stratospheric ozone transport. Finally, Section 4 discusses the main results and summarizes the conclusions of this study.

2. Data and Methods

2.1. Observations and Reanalysis Data

The BAyeSian Integrated and Consolidated ($BASIC_{SG}$; Ball et al., 2017, 2018) merged ozone data set is used for ozone observations. This data set merges the Stratospheric Water and OzOne Satellite Homogenized (SWOOSH) version 2.6 (Davis et al., 2016) and the Global OZone Chemistry And Related trace gas Data records for the Stratosphere (GOZCARDS) version 2.20 (Froidevaux et al., 2015, 2019). The $BASIC_{SG}$ method uses information from both data sets to account for and reduce artifacts arising from merging data from different instruments. For our study, monthly mean zonal mean ozone data on pressure levels covering the period January 1985–December 2018 have been used. $BASIC_{SG}$ covers the latitudinal range from 60°S to 60°N, with a horizontal resolution of 10° latitude, and has 27 vertical levels between 1 and 147 hPa (13–48 km), with a vertical resolution of 1.34 km.

For consistency with the SST data set prescribed in the REF-D1 simulations (described in Section 2.2), we use monthly mean SST data at 1° longitude-latitude resolution from the HadISST data set (Rayner et al., 2003) for the period 1960–2018. For the same reason, we employ the SOLARIS-HEPPA solar flux data set. also used to force the REF-D1 simulations. This data set is consistent with the historical forcing data set produced for CMIP6 (Matthes et al., 2017), but extended to the end of 2019 (More information can be found on https://solarisheppa.geomar.de/solarisheppa/ccmi2022). For surface temperature and zonal wind, we use monthly mean data from the ERA5 reanalysis (Hersbach et al., 2020). In order to calculate the residual stream function (ψ^*), we use daily mean data of the meridional component of the residual circulation ($\overline{v^*}$) derived from the ERA5 reanalysis (Serva, 2022). The stream function is obtained as

Table 1
List of the CCMI-2022 Models Used in This Study

Model	Reference(s)	Simulations		O_3, U, EESC	TEM data	AoA
		REF-D1	REF-D2			
ACCESS-CM2-Chem	Dennison and Woodhouse (2023)	3	1	✓	✓	----
CCSRNIES-MIROC3.2	Akiyoshi et al. (2023)	3	1	✓	✓	----
CESM2-WACCM	Gettelman et al. (2019)	4	3	✓	✓	✓[a]
CMAM	Jonsson et al. (2004) and Scinocca et al. (2008)	5	3	✓	✓	✓
CNRM-MOCAGE	Cussac et al. (2020) and Josse et al. (2004)	4	4	✓	----	✓
EMAC	Jöckel et al. (2016)	1	3	✓	✓	✓
GEOSCCM	Liu et al. (2022) and Oman et al. (2013)	1	----	✓	----	✓
LMDz6.2-LR-REPROBUS	Marchand et al. (2012)	1	----	✓	----	----
MIROC-ES2H	Kawamiya et al. (2020) and Tatebe et al. (2019)	----	3	✓	✓	✓
NIWA-UKCA2	Morgenstern et al. (2009)	3	3	✓	----	✓
SOCOL	Sukhodolov et al. (2021)	3	3	✓	----	✓[a]
UKESM1-StratTrop	Archibald et al. (2020) and Sellar et al. (2019)	3	----	✓	✓	✓

[a]In the CESM2-WACCM and SOCOL models, age of air data are only available in the REF-D1 simulations.

$$\overline{\psi^*}(\varphi,p) = \frac{-\cos(\varphi)}{g}\int_p^0 \overline{v^*}dp' \quad (1)$$

where p is pressure, φ is latitude, g the gravitational constant on Earth, and it is assumed that $\overline{v^*}$ tends to zero as $p \rightarrow 0$.

2.2. CCMI-2022 Model Simulations

We analyze output from 12 CCMs participating in the Chemistry Climate Model Initiative 2022 (CCMI-2022, Plummer et al., 2021). All the models, together with the ensemble size of each model and data availability, are listed in Table 1. We consider two different experiments available in CCMI-2022: historical simulations (REF-D1) and future projection simulations (REF-D2).

The REF-D1 historical hindcast simulations cover the period 1960–2018 and use forcings that closely follow the observed historical evolution. These simulations have prescribed monthly mean SST and sea ice cover (SIC) following the HadISST data set (Rayner et al., 2003). The quasi-biennial oscillation (QBO) should be nudged in all models, regardless of whether they are capable of internally generating a QBO or not, to ensure correct synchrony with the observations (Plummer et al., 2021). However, further analysis of the QBO in the REF-D1 simulations reveals that the QBO is not nudged, but internally generated, in some models (i.e., ACCESS, CNRM-MOCAGE, LMDz-REPROBUS, NIWA, and UKESM1; not shown), and thus, the modeled QBO phases are not synchronized with the observations. ODS follow the WMO-2018 baseline scenario (Carpenter et al., 2018; Plummer et al., 2021). Long-lived GHG are specified following the historical CMIP6 database (Meinshausen et al., 2017) until 2014, while they follow SSP2-4.5 scenario from 2015 to 2018 (Meinshausen et al., 2020; O'Neill et al., 2016).

Free-running simulations of the REF-D2 baseline projection span the period 1960–2100. They follow the SSP2-4.5 scenario of CMIP6 (Meinshausen et al., 2020; O'Neill et al., 2016) and the WMO-2018 baseline scenario for ODS. Note that in REF-D2 simulations, each model uses different SST and SIC. Some models are fully coupled to a 3-D ocean model (ACCESS, CESM2-WACCM, MIROC-ES2H, and SOCOL), while other models use prescribed SST and SIC provided by another simulation of an atmosphere-ocean coupled model from the same institution (MIROC3.2, CMAM, and CNRM-MOCAGE) or by a different coupled model from another institution from the CMIP6 archive (EMAC and NIWA). Regarding the model representation of the QBO, some models internally generate a QBO (ACCESS, GEOSCCM, LMDz-REPROBUS, MIROC-ES2H, and NIWA), but other models nudge zonal winds in the QBO domain (MIROC3.2, CESM2-WACCM, CMAM, EMAC, and SOCOL).

For comparison purposes, a set of REF-C2 long-term simulations from CCMI-1 is analyzed. The 15 CCMI-1 models used are (numbers in brackets indicate the ensemble size) as follows: ACCESS-CCM (2), CCSRNIES-MIROC3.2 (2), CHASER-MIROC (1), CMAM (1), EMAC-L47 (2), EMAC-L90 (1), GEOSCCM (1), HadGEM3-ES (1), MRI-ESM1 (1), NIWA-UKCA (5), SOCOL3 (1), ULAQ-CCM (3), UMSLIMCAT (1), UMUKCA-UCAM (2), and CESM1-WACCM (3). All the details of these simulations can be found in Morgenstern et al. (2017). They are analogous to the REF-D2 experiment but with the previous CCMI-1 baseline scenario RCP6.0 for long-lived GHG and WMO-2010 for ODS.

2.3. Statistical Analyses

Throughout this study, trends over the 1998–2018 period have been computed from a simple least squares linear fit of monthly deseasonalized time series for all variables, in contrast to Ball et al. (2018, 2019, 2020), who used a dynamical linear modeling (DLM) approach, or Godin-Beekmann et al. (2022), who used the LOTUS regression model (Petropavlovskikh et al., 2019). In our results, statistical significance is evaluated at the 95% confidence level ($p < 0.05$) using a Student's t test. Instead of computing a traditional multimodel mean with the trend of each simulation, we construct a probability density function following the methodology by Dietmüller et al. (2021) to get an estimate of the behavior of the multimodel trend. In this fashion, we have more complete information of the trends—and their uncertainties—across models, and we make a better comparison between REF-D1 and REF-D2 simulations and the observed trend values. To do so, we perform a bootstrap method as follows. First, we randomly choose one of the available models (m) and one of its ensemble members (e) if the model provides more than one simulation. Next, we calculate the linear regression slope coefficient ($T_{m,e}$) and its associated uncertainty ($\Delta_{m,e}$) for this model (m) and simulation (e) using the least squares method. Then, the computed ozone trend for this particular simulation is described as a normal distribution with mean $\mu_{m,e} = T_{m,e}$ and standard deviation $\sigma_{m,e} = \Delta_{m,e}$. Finally, a trend value within this normal distribution N ($\mu_{m,e}$, $\sigma_{m,e}$) is randomly selected. We repeat the above-explained process 10^6 times in order to have a large sample of simulated trends and build a robust probability distribution for the multimodel ozone trends.

3. Results

3.1. Assessment of Ozone Trends in CCMI-2022 Models Over the Period 1998–2018

The aim of this section is to analyze ozone trends for the 1998–2018 period in REF-D1 and REF-D2 CCMI-2022 simulations and to compare them with the observed ozone trends from the observational data set BASIC_{SG}. We select this period for several reasons—first, to be consistent with previous studies that used the same initial year; second, because ODS began to decline as a result of the Montreal Protocol around 1998; and finally, because the REF-D1 simulations only provide output up to the year 2018.

Figure 1 shows the latitude-pressure cross-section of the relative ozone trend over the period 1998–2018 for observations and the REF-D1 simulations, while Figure 2 shows trends for REF-D2 simulations. Overall, the spatial pattern and magnitude of trends in observations (green box in Figure 1) are highly consistent with those found in previous studies using different approaches and observational data sets (WMO, 2022). Upper stratospheric ozone (above 10 hPa) presents a consistent and almost hemisphere-symmetric increase in observations and in all model simulations. This behavior is associated with the reduction of ODS; thanks to the Montreal Protocol and also with a slowdown in ozone depletion reactions rates as the stratosphere cools due to the increase in GHG (Dhomse et al., 2018; Keeble et al., 2021; Oman et al., 2010; Portmann & Solomon, 2007). In the middle stratosphere (10–30 hPa), ozone trends are close to zero, so there is no overall change in this period.

More interestingly, observed LS ozone (below 30 hPa) shows a significant decrease peaking in the tropics and extending to the northern midlatitudes. Most of CCMI-2022 simulations (both REF-D1 and REF-D2) are not able to reproduce this observed pattern of ozone trends in the lower stratosphere, presenting large differences between simulations, even between different realizations of the same model, especially in midlatitudes. In the tropics, all the REF-D1 simulations exhibit negative trends in tropical LS ozone, in agreement with observations. As discussed in Introduction, these trends are associated with enhanced tropical upwelling due to increasing GHG (Dietmüller et al., 2021; WMO, 2022). However, only 8 simulations in REF-D1 (26% of the total) show a

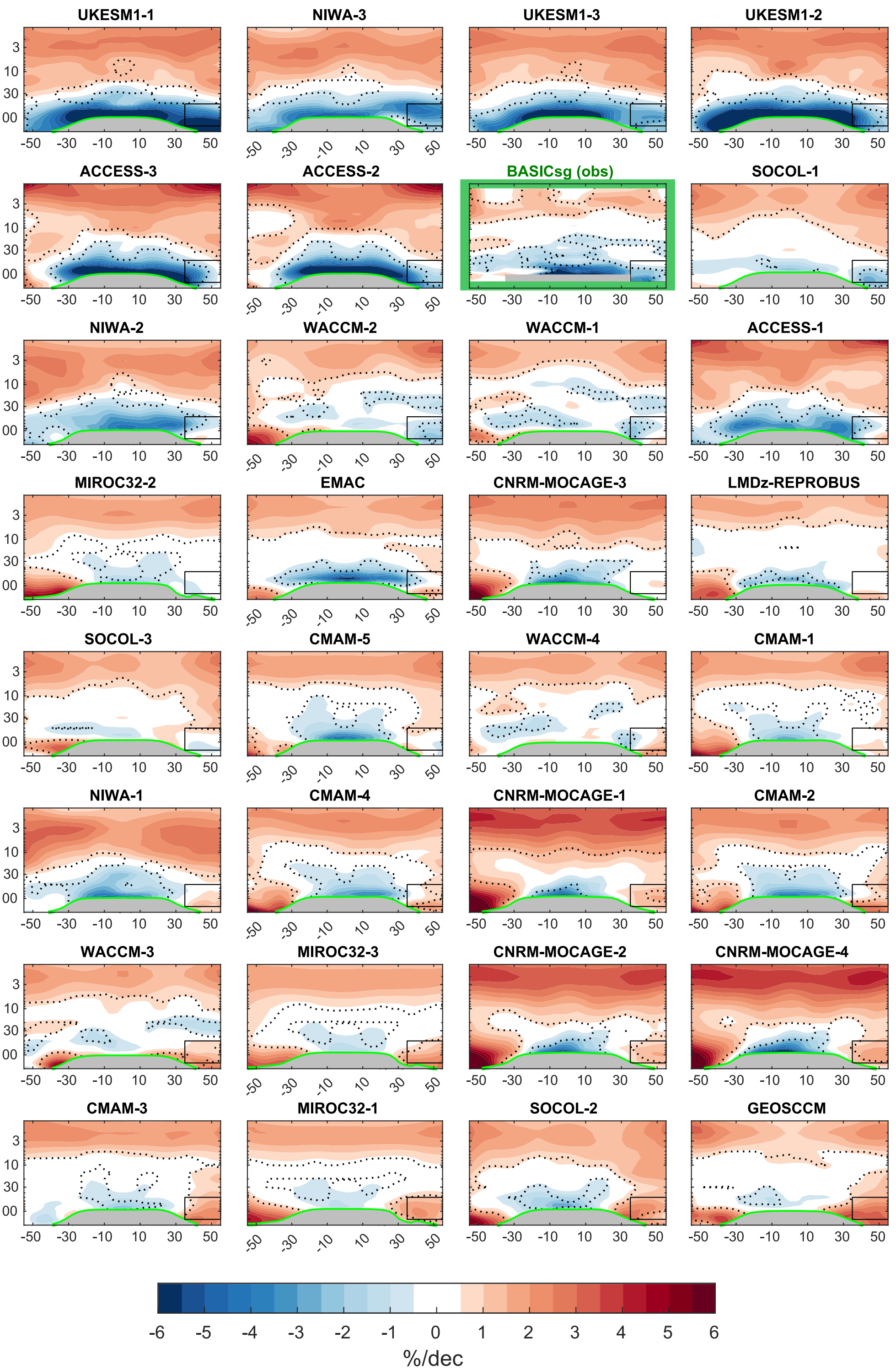

Figure 1. Latitude-pressure cross-section of the relative ozone trend in % per decade over years 1998–2018 from the observational data set BASICsg and all the REF-D1 simulations. The relative trend is calculated with respect to the 1998–2018 climatology. The simulations are ordered by the partial column ozone trend value in the northern midlatitudes lower stratosphere region (black boxes; 35°–55°N, 50–150 hPa). The numbers in the panel titles indicate the ensemble member. The WMO tropopause is indicated by the thick green line. Black dashed contours denote statistically significant trends at 95% confidence level (p-value <0.05). The green box marks the observations panel.

10.1029/2024JD042412

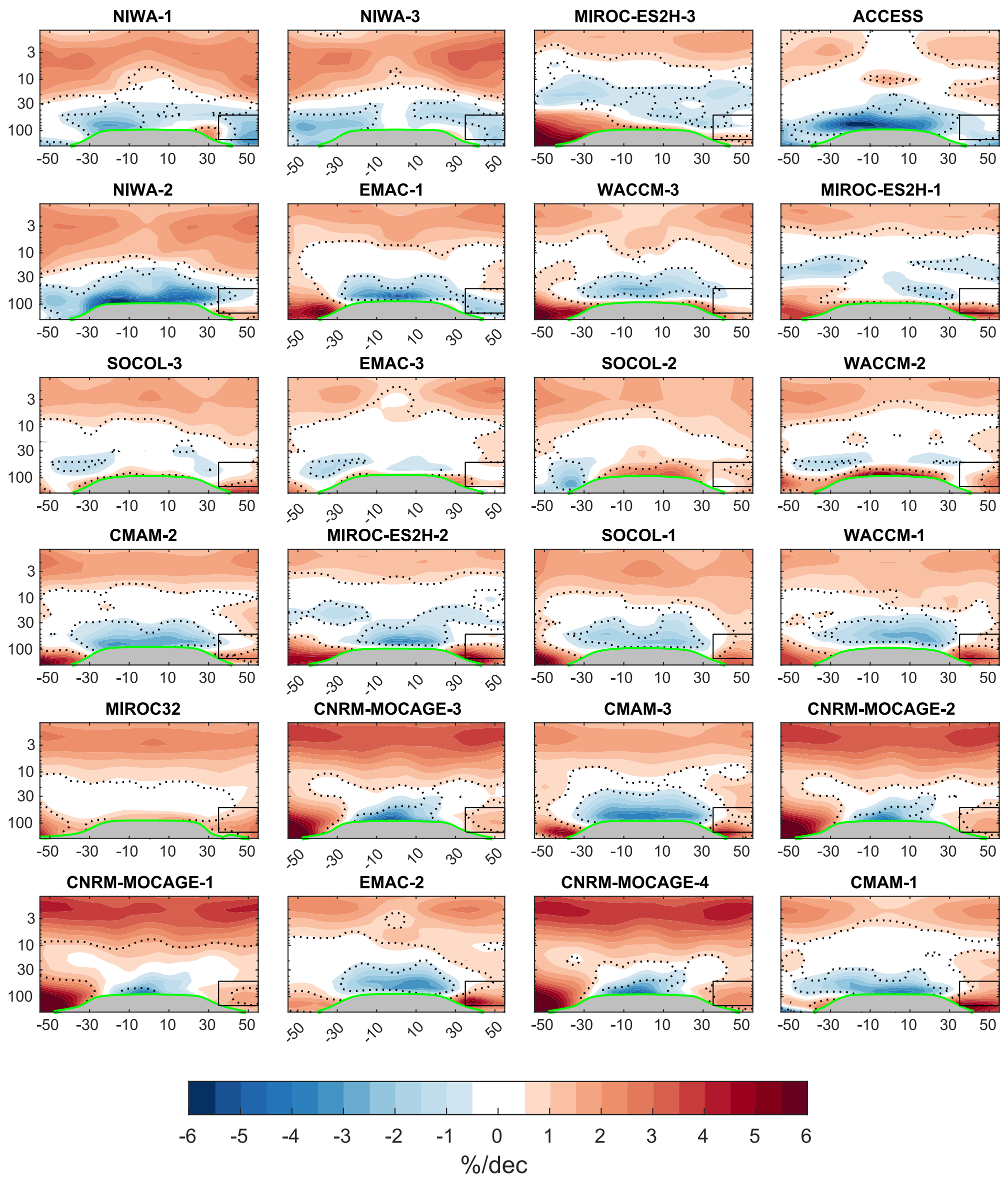

Figure 2. Same as Figure 1 but for REF-D2 simulations.

significant ozone decrease in LS ozone in the northern midlatitudes. For the REF-D2 simulations, most of the realizations also simulate ozone decrease in the tropics, although there are 3 simulations with positive ozone trends (MIROC3.2, WACCM-2, and SOCOL-2). In addition, only 2 simulations in REF-D2 (8%, NIWA-1 and NIWA-3) have significant negative ozone trends, both in the tropics and in the northern midlatitudes LS, in agreement with observations. The large intersimulation spread is dominated by intermodel differences, although in some cases, there are also major differences between realizations of the same model (e.g., WACCM, NIWA, and SOCOL).

It is important to keep in mind that there are some CCMs that use similar atmospheric components. Specifically, UKESM1 and ACCESS, which are two of the models that show the most negative trends in the lower stratosphere, are based on the same atmospheric model (MetUM-HadGEM3) and have similar chemistry. The NIWA-UKCA model, the other model with the most negative trends, uses an older version of the same atmospheric base model with a different dynamic core. The disagreement between observations and free-running models on LS ozone trends has been reported in previous studies using CCMVal-2 models (Ball et al. (2020) for the period 1998–2016) and CCMI-1 models (Dietmüller et al., 2021). None of the simulations analyzed in those studies were

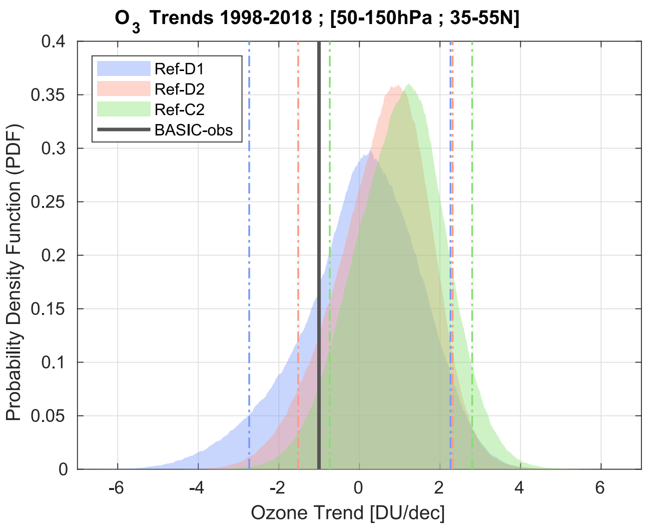

Figure 3. Probability density function of the northern midlatitudes LS partial column ozone trends for CCMI-1 REF-C2 simulations (in green), CCMI-2022 REF-D1 simulations (in blue), and CCMI-2022 REF-D2 simulations (in red). Dashed lines indicate the 5th and 95th percentiles of the distributions. The black line indicates the observational ozone trend value.

able to reproduce the LS ozone trend pattern, except for one simulation of UMUKCA-UCAM in the REF-B2 configuration (Ball et al., 2020). In contrast, in the new CCMI-2022, more simulations are able to reproduce, at least qualitatively, the observed trend pattern, and in particular, the ozone decrease in the northern midlatitudes.

In order to assess the degree of agreement between models and observations on northern midlatitudes LS ozone trends, we analyze the probability distributions of the simulated partial column ozone trend over the region 35°–55°N, 50–150 hPa (Figure 3, see Section 2.3 for details on the analysis). We compare the value of the observed trend (−1.00 ± 0.64 DU per decade) with all possible trends derived from different sets of model simulations. The most likely trend in the models is defined as the peak of the trend distribution (the mode of the distribution).

Although CCMI-2022 REF-D2 simulations show a preference for positive trends and REF-D1 for close to zero values, both the left tail and the mode of the distributions are shifted toward negative values compared to the previous REF-C2 CCMI-1 simulations. The ozone trend derived from the REF-D1 simulations, run with observed SST, is 0.19 DU per decade with a 90% confidence interval ranging between −2.71 and 2.26 DU per decade, while the most likely trend in the long-term REF-D2 simulations is 0.85 DU per decade ([−1.52, 2.30]). Thus, the observed trend (−1.00 ± 0.64 DU per decade) lies inside the 90% confidence interval for both sets of simulations in the CCMI-2022 models. In contrast, when compared to the CCMI-1 REF-C2 simulations, the observed trend lies outside the 90% confidence interval ([−0.93, 2.81]), consistent with Dietmüller et al. (2021). The slight improvement from the CCMI-1 REF-C2 simulations compared to the CCMI-2022 REF-D2 simulations is likely associated with improved boundary conditions and forcings in CCMI-2022 versus CCMI-1 rather than improvements in model formulation, as some models have minimal changes between CCMI-1 and CCMI-2022 versions.

The comparison between REF-D1 and REF-D2 trend distribution reveals a better simulation of midlatitudes LS ozone trends in the former. The observed trend can be considered as a plausible realization within REF-D1 simulations (24th percentile, the observed value is almost within the 50% central values of the distribution), while it would be an extreme though possible realization for REF-D2 simulations (9th percentile). It is important to point out that not having the same models in the REF-D1 and REF-D2 groups can affect our results. In particular, the UKESM1 model, which shows the most negative trends in the tropics and midlatitudes in REF-D1, did not have REF-D2 simulations available at the time of this study. When we computed the trend distributions including only the models that provide data for both experiments, our results still hold the following: both the mode and the left tail of the REF-D1 distribution shifts to more negative values, and thus, the mode is closer to the observations in REF-D1 than in REF-D2 (Figure S1 in Supporting Information S1).

Using the same approach, Figure 4 displays the comparison of the ozone profile trends between models and observations. The trend value for REF-D1, REF-D2, and REF-C2 is calculated as the most likely trend value of the trend probability distribution for each pressure level (see Section 2.3 for more information); the 90% confidence interval for REF-D1 trend distribution is shown by the blue envelope. Consistent with previous studies using observational data sets and older CCMI simulations (Godin-Beekmann et al., 2022; Petropavlovskikh et al., 2019), there is good agreement in the magnitude of ozone increase in the upper stratosphere (above 10 hPa) between observations and models, both in the tropics and midlatitudes. In particular, the similarity between the REF-D1 and REF-D2 simulations confirms that in the upper stratosphere, trends are due to long-term (externally forced) changes and are not affected by interannual natural variability.

In the lower stratosphere, as expected from Figures 1–3, the observed and simulated ozone trend values diverge, but to different degrees depending on the region and the type of simulation, and with large uncertainties in the trend value. The agreement is better in the tropics, where CCMs and observations show negative trends, albeit with an underestimation by the models below 50 hPa, especially for the REF-C2 and REF-D2 simulations. For the REF-D1 experiment, the simulated negative trend is closer to the observed value, and when taking into account the large intermodel uncertainty, the REF-D1 trend is consistent with observations. In the northern midlatitudes,

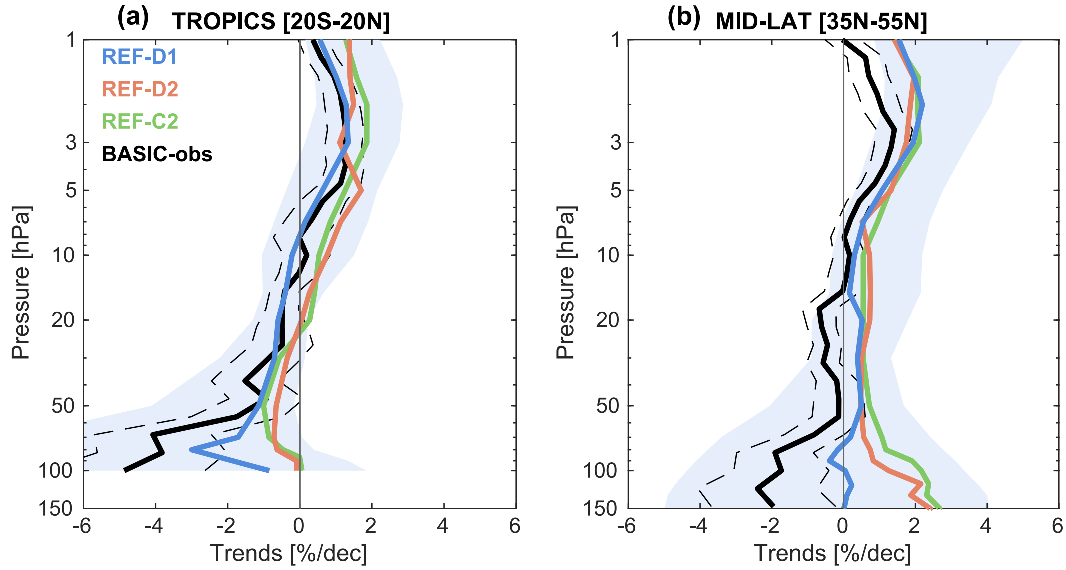

Figure 4. Stratospheric ozone profile trends in (a) the tropics (20°S–20°N) and (b) northern midlatitudes (35°N–55°N), for REF-C2 (in green), REF-D1 (in blue), REF-D2 (in red), and BASIC observations (in black). The trend value for each set of simulations is the most likely trend value of the trend probability distribution for each level pressure. Dashed black lines indicate the uncertainties in the observed trend. Blue shaded areas represent the 90% confidence interval for REF-D1 distribution.

the difference between observed and simulated trends is larger, although the improvement in the simulation of trends when part of the natural variability is prescribed is confirmed, as the ozone trend value in REF-D1 is closer to observations than in REF-C2 and REF-D2. When the ozone profile trends are computed using a traditional multimodel mean instead of the "most likely trend" method (not shown), our conclusions remain valid.

To investigate if REF-D1 simulations also reproduce the ozone trend pattern better than REF-D2 simulations, and not just the trend value in the lower stratosphere, we next analyze the relationship between trends in the northern midlatitudes region and the spatial pattern of trends. For this purpose, Figure 5 shows the across-simulation correlation coefficients between local ozone trends and northern midlatitudes LS (35°–55°N, 50–150 hPa region) partial column ozone trend. Focusing on the lower stratosphere, the main differences between the REF-D1

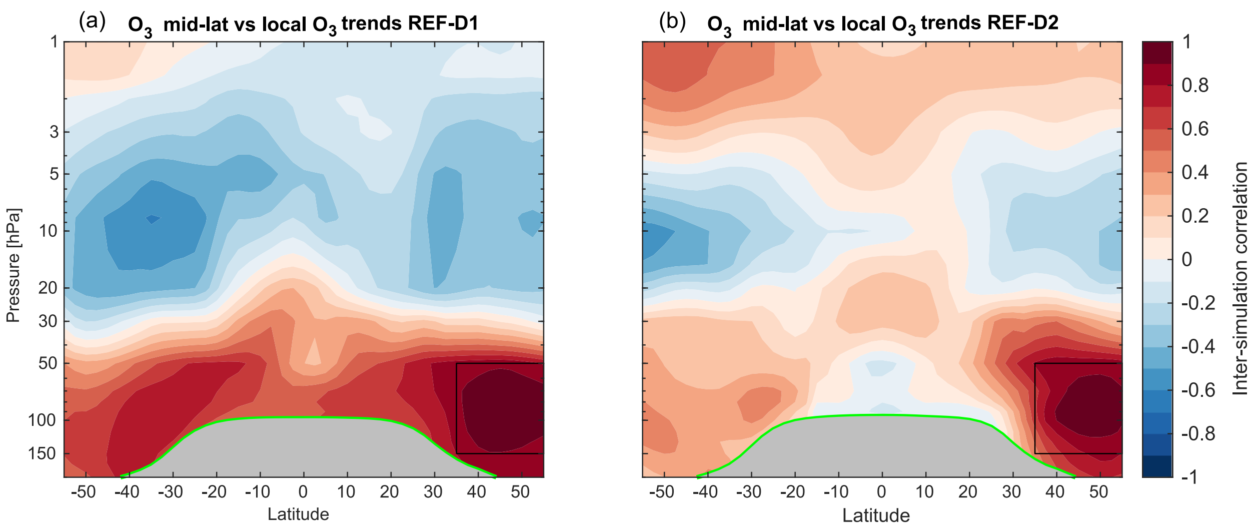

Figure 5. Correlation coefficients between midlatitudes LS partial column ozone trends integrated over the box shown in black and local ozone trends at each point across simulations for (a) REF-D1 and (b) REF-D2. The black box indicates the region where midlatitude LS ozone is integrated. The tropopause is indicated by the thick green line.

and REF-D2 patterns appear in the tropics. In the REF-D1 simulations (Figure 5a), the intersimulation correlation between tropical and midlatitude LS ozone trends is positive, with values around 0.5–0.6. This correlation indicates a link between trends in the midlatitudes and tropical lower stratosphere consistent with the observed trends, which feature the same sign in the tropics and midlatitudes (and opposite sign with respect to trends in the middle and the upper stratosphere). In contrast, REF-D2 simulations present near-zero intersimulation correlation between tropical and midlatitude LS ozone trends. This result was previously highlighted by Dietmüller et al. (2021) for REF-C2 simulations, although the correlation they found was slightly more negative.

In summary, the analysis above (Figures 1–5) shows that overall, the new set of CCMI simulations has an improved representation of LS ozone trends, but yet only a few simulations are able to correctly reproduce the observed trends. The comparison between historical hindcast simulations (with prescribed observed SST and SIC, REF-D1) and the coupled simulations (REF-D2) indicates that when at least part of the natural variability is prescribed, the models are able to reproduce LS ozone trends more accurately. Interestingly, there is a large spread among simulations not only in REF-D2 but also in REF-D1, suggesting an important role of internal atmospheric variability for trends over the shorter period. To investigate this further, the next section analyzes how natural and forced variability contribute to the midlatitude LS ozone trends.

3.2. Contribution to Lower Stratospheric Ozone Trends From Natural and Forced Variability

To quantify the contribution of different modes of climate variability, as well as different external forcings, to the midlatitudes LS ozone trends (partial column integrated over the region 35°–55°N, 50–150 hPa), we perform the following multiple linear regression (MLR) including terms to account for both the influence of natural variability and the forced response to GHGs and ODSs:

$$O_3(t) = \alpha_1 \cdot \mathrm{QBO}_1(t) + \alpha_2 \cdot \mathrm{QBO}_2(t) + \alpha_3 \cdot N_{3.4}(t) + \alpha_4 \cdot f_{10.7}(t) + \alpha_5 \cdot \mathrm{GW}(t) + \alpha_6 \cdot \mathrm{EESC}_{50hPa}(t) + \epsilon(t). \quad (2)$$

In Equation 2, QBO_1 and QBO_2 are indices corresponding to the first two empirical orthogonal functions (EOFs) of the zonal wind between 5°S and 5°N over the layer 10–70 hPa (Wallace et al., 1993), $f_{10.7}$ is the 10.7-cm solar radio flux used as proxy for the 11-year solar cycle, and $\mathrm{N}_{3.4}$ is an ENSO index with the standardized SST anomalies in the Niño3.4 region (5°N–5°S, 170–120°W). We consider these sources of natural variability because previous work has shown that they strongly affect stratospheric ozone (Benito-Barca et al., 2022; Diallo et al., 2019; Randel & Wu, 2007; Wang et al., 2022; Xie et al., 2020). Volcanic effects have not been included as no major volcanic eruptions have occurred in the period 1998–2018. The forcing response to GHG is assessed with a global warming index (GW), calculated as the area-weighted global mean surface temperature (*ts*). The ODS signal is evaluated using the area-weighted global mean equivalent effective stratospheric chlorine (EESC) at 50 hPa (EESC_{50}). EESC is a convenient metric to quantify the effects of halogens (chlorine and bromine) on stratospheric ozone depletion (Newman et al., 2007). The residual is denoted by ϵ(t). All indices have monthly frequency and have been deseasonalized before including them into the regression model.

The analysis of the contribution to LS ozone trends from each term included in Equation 2 has been carried out as follows. First, the coefficients associated with each regressor (α_i) are obtained by performing the MLR for the period 1960–2018. Then, the time series of ozone associated with each proxy is calculated by multiplying the coefficient by the time series of the index. Finally, the linear trend of the time series is calculated over the period 1998–2018 using a least square linear fit. The second column of Figure 6 displays the trend of the original midlatitude LS ozone series for each REF-D1 simulation, while the remaining columns show the contribution to the trend of each of the different regressors. Note that the QBO column is the sum of the contributions related to the QBO_1 and QBO_2 indices.

Overall, the linear effects of natural variability associated with the QBO and ENSO have a small contribution to the ozone trend in this period. The trend associated with the QBO is negative and smaller (in absolute value) than 0.20 DU per decade in all simulations that have the QBO nudged to the observed. The negative sign is due to the fact that during the easterly phase of the QBO, there is more ozone in midlatitudes than during the westerly phase (Wang et al., 2022), and 1998 is an easterly phase year, and in 2018, the westerly phase begins. The trend related to ENSO is slightly positive in all simulations and in observations, conditioned by the low ozone values associated with the 1998/2000 La Niña and the high values associated with the 2015/16 El Niño in relation to the ozone transport toward midlatitudes by the residual circulation of the shallow branch and two-way mixing (Benito-

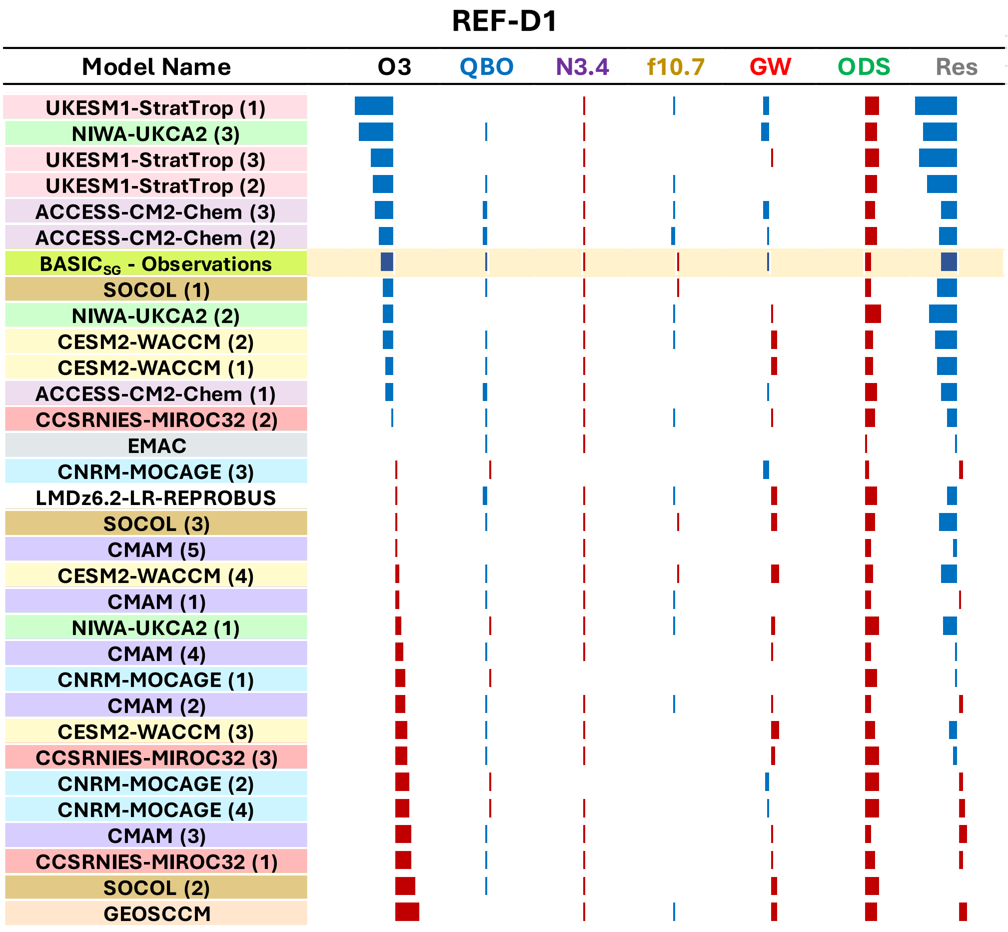

Figure 6. Decomposition of the northern midlatitudes LS (35°–55°N, 50–150 hPa) ozone trends in the period 1998–2018 into the contribution of the different explanatory variables used in the MLR for REF-D1 simulations. In the first column, the number in parentheses indicates the ensemble member. The limits in each column range from −3.5 to 3.5 DU per decade. The yellow-shaded row corresponds to the observed trend. The last column shows the trend of the MLR residual.

Barca et al., 2022; Calvo et al., 2010). Regarding the solar cycle, the associated ozone trend is very slightly negative in most of the simulations. When the analysis is performed with the REF-D2 simulations (Figure S2 in Supporting Information S1), with each model having different QBO and ENSO phases, the same conclusion is reached: the trends associated with the linear response to these natural variability modes are small, and there are no significant differences between simulations.

The ozone trend induced by global warming is given by column "GW" in Figure 6. The models disagree on the sign of the response in this short period. However, in all simulations, the trend is smaller in absolute value than 0.5 DU per decade, and therefore of low relevance for explaining ozone trend values. This result is in good agreement with the findings of Dietmüller et al. (2021), who showed, using CCMI-1 sensitivity simulations, that global warming has a minor net role in the ozone trend in the midlatitude lower stratosphere in the period 1998–2018.

As expected, the trend associated with the reduction of ODS in the stratosphere from 1998 onward is consistently positive in all simulations and also in observations, with values even above 1 DU per decade. This maybe due to the reduction in local ozone depletion following the ODS decrease or to ozone transport from the upper stratosphere, where ozone increases strongly during this period. The ozone increase caused by the decrease in ODS may explain why there are simulations showing positive trends in this period. Following this, Dietmüller et al. (2021) indicated that positive midlatitude LS ozone trends simulated in CCMI-1 models come mainly from changes in ODSs and that a potential overestimation of this effect in models could lead to disagreement with the observations. Accordingly, our results show that the ODS-driven ozone recovery in observations is lower than in most

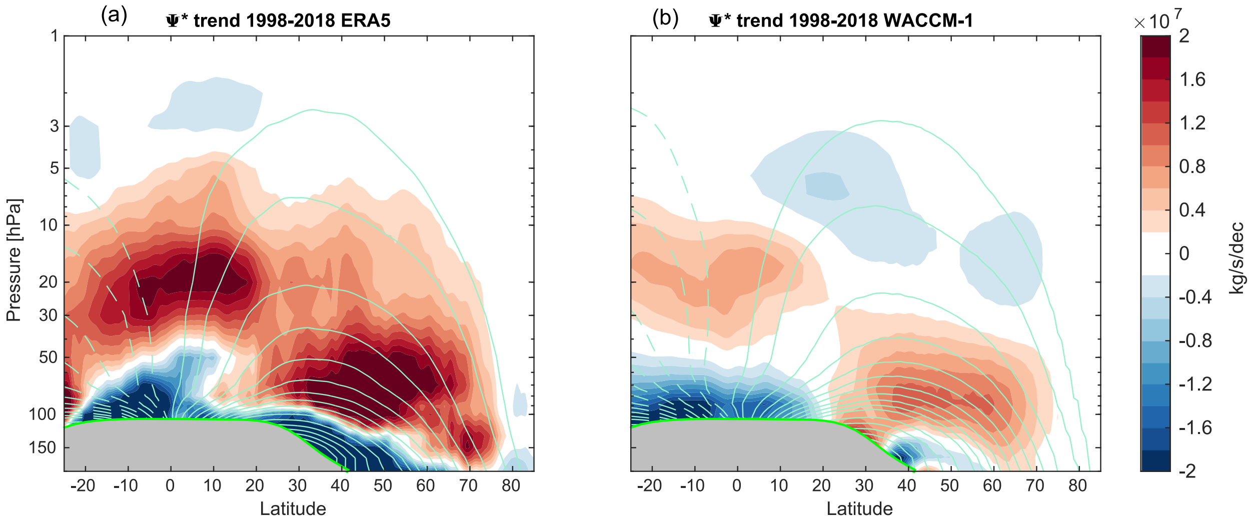

Figure 7. Latitude-pressure cross-section of the residual stream function (Ψ*) trend in kg/s per decade over years 1998–2018 (color shading) from (a) ERA5 and (b) WACCM-1 simulation. Green contours show 1998–2018 climatology of Ψ*. Contours are drawn every 10^8 between ±10^9 and every 2 × 10^8 in the rest. The tropopause is indicated by the thick green line.

models. However, note that this ODS-driven ozone recovery in observations is not consistently lower in the simulations with the most negative ozone trends, so this hypothesis is rejected. Moreover, there are no major differences in this contribution between REF-D1 simulations, suggesting that ODS-related trends cannot explain the wide spread found in the simulated ozone trends.

In fact, Figure 6 clearly shows that the differences between simulations mainly come from the trends of the regression residuals, which are either negative or slightly positive and clearly correlated with the overall trend. The simulations in which the trend of the residual is most negative are those with the largest net ozone reduction. This residual may include several factors not included in the regression. For instance, given the linear nature of the analysis, the residuals could be related to nonlinear effects of the natural variability modes included in the linear regression, nonlinear effects of the ODS and GHG or their interaction with natural modes, or other natural variability not included in the MLR. Another possibility is that the residuals are linked to internal variability not included in the MLR related to dynamical transport of ozone. As mentioned in Introduction, several studies have suggested that the spread in simulated ozone trends stems from differences in ozone transport trends and dynamical variability in each model. Thus, in the following section, we study the relationship between mid-latitudes LS ozone trends and changes in stratospheric ozone transport (and their variability) in more depth.

3.3. How do Changes in Transport Processes Affect Recent Trends in Lower Stratospheric Ozone?

The global distribution of stratospheric ozone is controlled by advection due to the residual circulation, by two-way mixing following Rossby wave dissipation, as well as by chemical production and loss (Abalos et al., 2013; Garcia & Solomon, 1983; Plumb, 2002). Hence, trends in ozone are expected to be controlled by changes in the residual circulation, changes in mixing, and also changes in chemistry through changes in concentration of other chemical species and stratospheric temperatures. The chemistry-driven trend has been discussed in the previous section, analyzing the contribution of the ODS. In this section we aim to explore how transport processes affect recent trends in lower stratospheric ozone.

First, we study residual circulation changes in the period 1998–2018. Using a replay simulation of GEOS nudged to the MERRA-2 reanalysis, Orbe et al. (2020) found that the negative ozone trend in the Northern Hemisphere lower stratosphere is associated with a poleward expansion of the residual circulation in the lower stratosphere, with downwelling reduced in the subtropics and enhanced at higher latitudes. They noted that opposing effects of mixing played negligible role for the ozone trends. Figure 7a shows the residual stream function (Ψ*) trend for ERA5 reanalysis over the 1998–2018 period. Focusing on the Northern Hemisphere, the positive trend centered north of turnaround latitudes (maxima in the streamlines) below 50 hPa indicates a poleward expansion of the shallow branch of the residual circulation, consistent with the results of Orbe et al. (2020). The poleward expansion of the shallow branch implies that the streamlines are stretched northward, because the Ψ* positive trend is larger north of the turnaround latitudes than south of them. This stretching generates an increase in poleward horizontal transport in the region of interest (∼35–60°N) and a reduction in downwelling just north of the turnaround latitudes. When we carry out this analysis in the REF-D1 simulations, we find that some simulations are capable of reproducing a similar behavior. In particular, Figure 7b displays the Ψ* trend for the first ensemble member of the WACCM model (WACCM-1), which presents the Ψ* trend pattern that qualitatively resembles ERA5: positive trend north of the turnaround latitudes, indicating the poleward expansion of the shallow branch. The reduced downwelling and the enhanced poleward transport drive the reduction of ozone advection into the midlatitudes lower stratosphere (not shown). However, the Ψ* trend amplitude is much smaller in WACCM-1 than in ERA-5, consistent with the results presented in Orbe et al. (2020) using MERRA-2 reanalysis and free-running simulations of the GEOSCCM model. Note that this WACCM-1 realization also presents an ozone trend pattern that resembles observations at midlatitudes (see Figures 1 and 6), although its magnitude is smaller, likely due to the smaller amplitude of the Ψ* trend. These similarities support the hypothesis of the poleward expansion of the shallow branch as a potential driving mechanism for negative ozone trends over this period. If we look the Ψ* trends in the other WACCM ensemble members, we find notable differences between them, which is consistent with the large intermember variability observed in the WACCM model also in the ozone trends (see first column of Figure 6). These large differences between members highlight the important role of internal variability in the trends over a shorter period such as 1998–2018 and again confirm that the trend is not an externally forced change.

In Section 3.2, we hypothesized that the intersimulation spread in ozone trends may result from differences in transport trends. To explore this, Figure 8a shows the point-by-point correlation between stratospheric mean age of air (AoA) trends and ozone trends across a subset of 13 REF-D1 simulations with available data (WACCM-1/4, CMAM-1/5, EMAC, and UKESM1-1/3; see Table 1). AoA is defined as the transit time of an air parcel since its entry into the stratosphere through the tropical tropopause and provides an integrated measure of stratospheric transport (Waugh & Hall, 2002). Focusing on the lower stratosphere, we find high positive correlation values, larger than 0.8, in the tropics and northern midlatitudes. This confirms that intersimulation differences in ozone trends are highly influenced by differences in transport trends. The positive correlation in the tropics is consistent with the well-known relationship between ozone and upwelling trends. Increased upwelling raises younger, ozone-poor air parcels from the tropical tropopause, leading to negative trends in both AoA and ozone. To further study the positive correlations in midlatitudes, we analyzed the relative role of residual circulation and two-way mixing on the spread in ozone trends in the midlatitude region.

Figures 8b and 8c display the correlation between ozone trends and the residual circulation transit time (RCTT) and aging by mixing (AbM) trends, respectively. RCTT is the transit time of hypothetical transport only by the residual circulation, so lower RCTT values means faster residual circulation. RCTT is calculated from the backward trajectories driven by the monthly mean TEM residual circulation ($\overline{v^*}, \overline{w^*}$) in the latitude-height plane with a standard fourth-order Runge-Kutta integration. The backward trajectories end at the thermal tropopause, and the elapsed time is the RCTT. AbM is the difference between AoA and RCTT, quantifying the effect of two-way mixing in the AoA, which is typically aging air parcels due to recirculation in the stratosphere (Garny et al., 2014). This term actually includes mixing on resolved scales and additional effects of mixing processes on unresolved scales (namely parametrized and numerical diffusion). For more details on RCTT and AbM, we refer to Birner and Bönisch (2011), Dietmüller et al. (2017), and Garny et al. (2014).

In the tropical lower stratosphere, RCTT trends correlate positively with ozone trends with correlations larger than 0.8 extending up to 40°N. In the midlatitude region, we find that RCTT and ozone trends are positively correlated in the lowermost stratosphere, whereas negative correlations, albeit weaker, appear above 70 hPa. This dipolar pattern in midlatitudes suggests that both the shallow and deep branches of the residual circulation influence ozone trends. Positive correlation at lower levels can be associated with the shallow branch, indicating that a stronger acceleration of the circulation leads to more negative ozone trends in the region, as younger, ozone-poor air is transported from the tropical tropopause to midlatitudes. In contrast, the negative correlation at upper levels is related to downwelling from the deep branch of the residual circulation, because an enhancement of the circulation not only brings younger air from tropics to extratropics but also ozone-rich air from the middle stratosphere. Moreover, two-way mixing effects are also important as shown in Figure 8c. The correlation between AbM and ozone trends in the midlatitudes LS is positive but with large differences between the equatorial

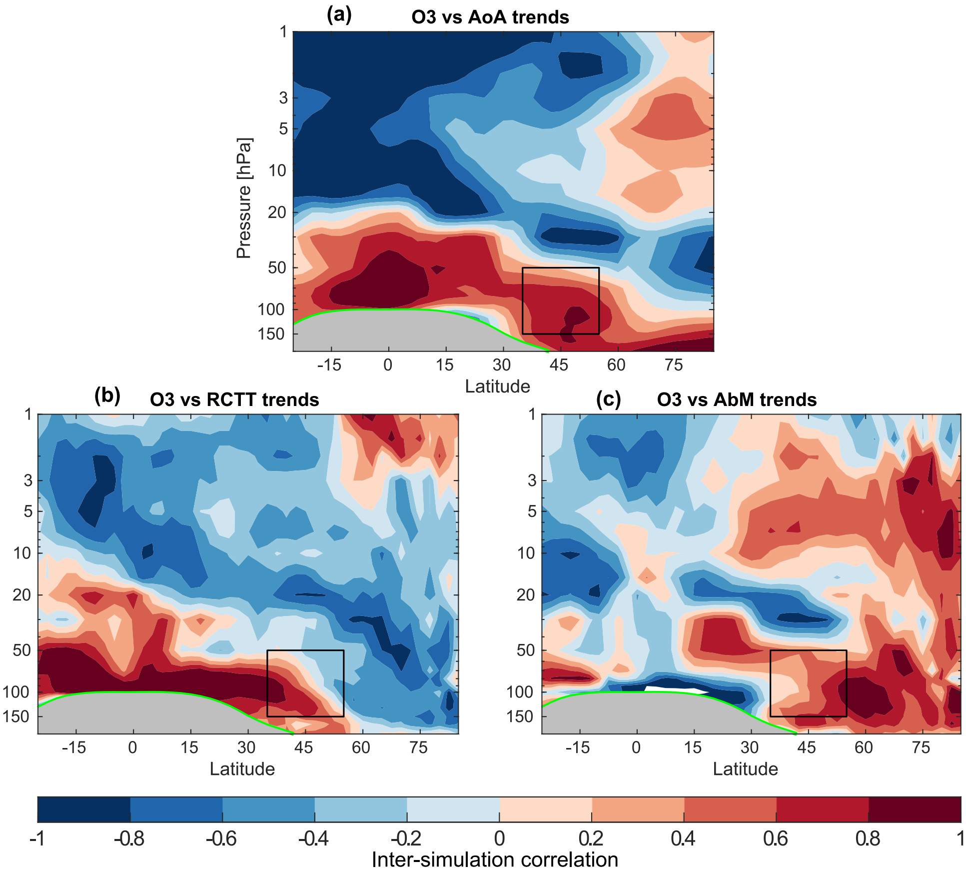

Figure 8. Point-by-point correlation between local ozone trends and (a) local AoA trends, (b) local RCTT trends, and (c) local AbM trends across a subset of 12 REF-D1 simulations (WACCM-1/3, CMAM-1/5, EMAC, and UKESM1-1/3). The black box represents the northern midlatitudes region (35°–55°N, 50–150 hPa). The tropopause is indicated by the thick green line.

and polar flank. This gradient suggests that the midlatitudes LS region is affected by two-way mixing between tropics and extratropics, which reduce ozone not only in midlatitudes but also between midlatitudes and the polar region, increasing ozone in our region of interest. Overall, Figure 8 reveals that the northern midlatitudes LS is a complex region, influenced by many competing transport processes connected to both the tropics and the polar region. Therefore, the different balance between them results in the intermodel differences in the LS ozone trends.

To further explore the differences across models in ozone transport, the interannual point-by-point correlation between ozone and AoA is shown in Figure 9. Because in this analysis the differences between different simulations of the same model are negligible, Figure 9 shows only the first ensemble member for each model. There are clear intermodel differences, indicating that the transport-ozone covariability is different in each model. In particular, the UKESM1 and NIWA models, which show the most negative trends in ozone, feature the weakest interannual covariability between ozone and AoA in the lower stratosphere. The different relationship between ozone and transport reflects a different ozone response to the dynamical variability across the models, which may help explain the large intermodel differences in ozone trends. An analysis of the standard deviation of ozone concentrations shows the different internal variability of ozone across models, with ACCESS, NIWA, and UKESM1 models showing the largest variability and MIROC3.2 and CMAM the weakest (not shown).

4. Conclusions and Discussion

We present here an updated analysis of recent trends in LS ozone, motivated by previous results highlighting the lack of ozone recovery and the disagreement between observations and model trends in this region (WMO, 2022, and references therein). The main novelty of our study is that we use simulations with prescribed SST from observations covering the period 1998–2018 in addition to simulations run with modeled ocean, which allows us

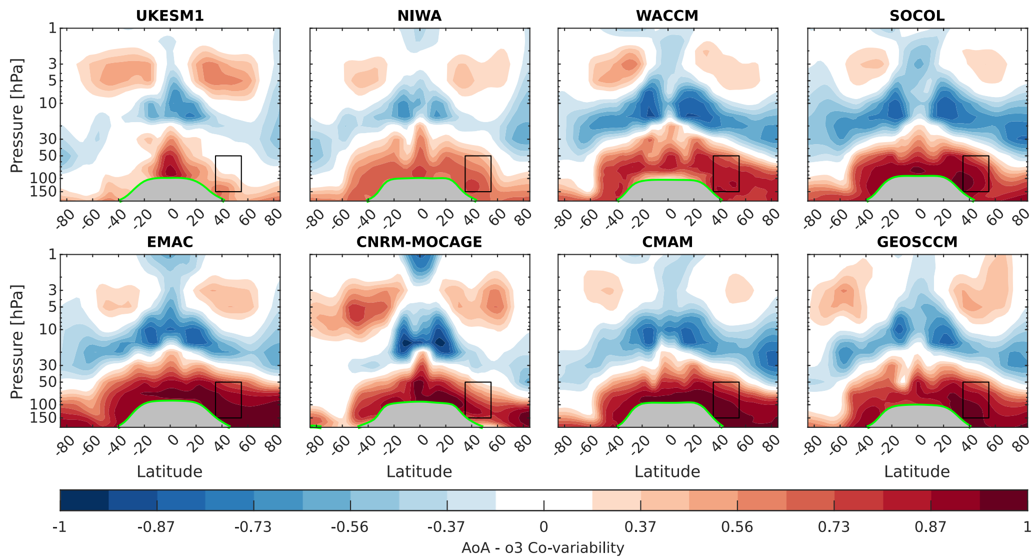

Figure 9. Interannual correlation between AoA and ozone for the model ensemble member #1 for REF-D1 simulations. The black box represents the northern midlatitudes region (35°–55°N, 50–150 hPa). The tropopause is indicated by the thick green line. The models are sorted by their first occurrence of any ensemble member in the first column of Figure 6.

to better address the role of natural variability on the recent ozone trends. The main findings of our study are summarized as follows:

- LS ozone trends over the period 1998–2018 are better represented by CCMI-2022 models than by previous generations of chemistry-climate models, likely because of improved boundary conditions and forcings in CCMI-2022 compared to CCMI-1 rather than improvements in their model formulation. In the tropical lower stratosphere, almost all models simulate negative trends over this period, consistent with the observed trend sign, albeit with a slight underestimation of its magnitude. In the northern midlatitudes, there are still few simulations able to reproduce the observed negative trends. Moreover, there is large intersimulation spread, highlighting the important role of internal variability in the trends over a short period such as 1998–2018.
- The observed trend pattern in the lower stratosphere is better simulated in models when the SST are prescribed to the observations (REF-D1 simulations) than when the SST are modeled (REF-D2). This finding supports the hypothesis from previous studies that natural variability, and in particular, associated with SST variability, has an influence on ozone trends over a short period such as 1998–2018. However, the influence of this natural variability cannot be described as the linear response to the main climate variability modes (ENSO and QBO), which make a small contribution to the ozone trend over this period.
- The ozone trend associated with the decrease in ODS is consistently positive in all simulations. Our results show that the response to ODS cannot explain the intermodel differences in recent trends and discard the possibility that an overestimation of the response to ODS in models could account for the disagreement with the observations.
- Observed changes in the residual circulation suggest a poleward expansion of the shallow branch as a potential dynamical mechanism for the negative ozone trend in midlatitudes. We show that one simulation is able to reproduce the observed change in both ozone and residual circulation, and the fact that other members of the same model feature completely different trends confirms the key role of internal variability.
- Differences in the representation of ozone transport internal variability across models play a major role in the intersimulation spread in ozone trends. The midlatitude lower stratosphere is a particularly complex region affected by multiple competing transport processes. The model representation of these processes and their impact on ozone (advection by the shallow and deep branches of the residual circulation and two-way mixing with tropics and the polar region) and their internal variability are crucial to determine the ozone trends over a shorter period.

We acknowledge that our analysis based on a multiple linear regression cannot fully clarify the role of natural variability as it does not consider nonlinear effects. For instance, ozone trends in midlatitudes can be affected by

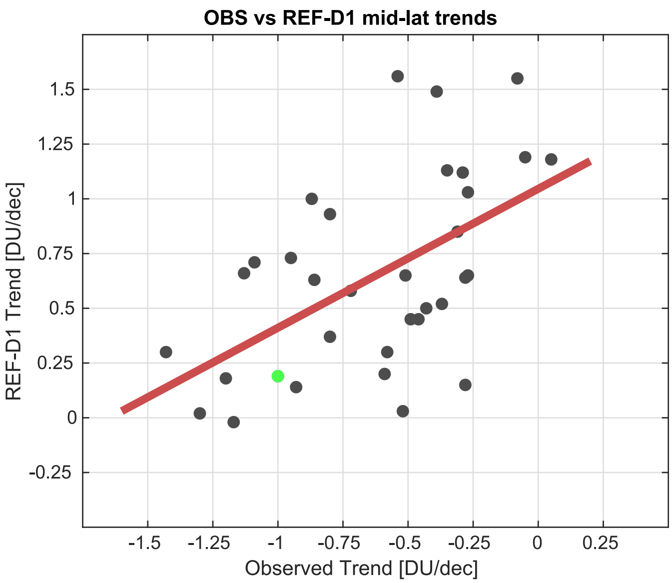

Figure 10. Scatterplot of northern midlatitude LS ozone trend for REF-D1 simulations (vertical axis) versus observations (horizontal axis) for varying start years from 1994 to 2000 and end years from 2014 to 2018. The REF-D1 trend is calculated as the peak of the REF-D1 trend probability distribution (see Section 3.1 and Figure 3 for more information). The green point represents the value for the period 1998–2018. The least squares fit is shown by the red line.

the QBO through QBO-induced secondary circulation and also through QBO seasonal-depending interactions (Ball et al., 2019). Moreover, linear and nonlinear interactions between the QBO and ENSO signals have been previously reported (Xie et al., 2012, 2020).

We have argued that when SSTs are prescribed to observations in models, the simulation of the observed ozone trend in the lower stratosphere is significantly improved, highlighting that natural variability plays an important role in ozone trends. However, this does not necessarily mean that the influence of natural variability is correctly captured in the models. A preliminary check is presented in Figure 10. This figure shows the midlatitudes LS ozone trends for varying start years between 1994 and 2000 and end years between 2014 and 2018 for observations and REF-D1 simulations, in which the SST follows the observations. Although trends for REF-D1 simulations show a preference toward positive values for all periods compared to observations, the variations of the simulated trends for different periods are consistent with variations of the observed trends for the same periods (Spearman's correlation value of $\rho = 0.56$). Thus, this preliminary analysis suggests that the influence of natural variability on the simulated trends is consistent with the observations. However, the slope of the linear fit is different from 1, which could indicate possible model problems. Overall, the assessment of how well the influence of natural variability on ozone and transport is represented in the CCMI-2022 REF-D1 simulations requires a more in-depth analysis.

One of the findings of the paper is the identification of a poleward expansion of the residual circulation as a potential driving mechanism for negative ozone trends over 1998–2018. This was previously proposed by Orbe et al. (2020), who also showed that the free-running simulations of the GEOSCCM model produced weaker residual circulation and ozone changes over the period 1998–2018 than MERRA-2 and ERA-Interim reanalysis. This also occurs in our study, as the changes in the residual circulation in the ERA-5 reanalysis (and the associated ozone trend in the observations) are larger than those shown by the WACCM-1 REF-D1 simulation. Much larger residual circulation changes in reanalyses (MERRA-2, ERA-Interim, and ERA-5) than models could indicate problems in calculating a highly derived quantity like Ψ^* in reanalysis, which might produce spurious trends. However, MERRA and ERA families of reanalysis employ completely different assimilation systems, which makes unlikely that this would be the actual reason for the differences between reanalyses and models. Thus, one emerging possibility could be the difficulty in the models to correctly reproduce changes in the large-scale circulation, and in particular, changes in the lower stratospheric residual circulation. Future research is needed to determine why reanalyses produce much larger residual circulation trends than free-running models and how this affects trends in lower stratospheric ozone.

Finally, we note that models that simulate negative midlatitudes ozone trends (i.e., UKESM1, NIWA-UKCA2, and ACCESS-CM2) are not necessarily those that reproduce stratospheric dynamics more realistically. As noted in Section 2.2, the QBO in these models does not follow the observed phases in the REF-D1 simulations. Furthermore, UKESM1 and NIWA-UKCA2 have an unrealistic representation of the mean wintertime polar vortex in the period 1998–2018, with winds that are up to 35% stronger than ERA-5 (not shown). This can affect ozone trends indirectly through two-way mixing, as the polar vortex acts as mixing barrier, and could also be an indication of unrealistic wave activity, affecting the residual circulation. In addition, we have found that the UKESM1 model presents too young AoA values compared to the rest of the models, mainly due to a too low AbM compared with the other models (not shown). In this sense, it would be interesting to study different transport diagnostics, such as passive tracers with multiple timescales, to evaluate how the CCMI-2022 models reproduce transport. Unfortunately, these diagnostics have not been produced by most CCMI-2022 models. We encourage modeling centers to produce a broad range of passive tracers spanning multiple sources and timescales in order to perform more in-depth studies of transport in these types of models.

Overall, our results show that the observed negative ozone trends in the midlatitudes lower stratosphere are a plausible realization for state-of-the-art chemistry-climate simulations given the observed boundary conditions, and result from internal variability rather than being externally forced. On the other hand, our study finds substantial discrepancies in the ozone transport variability across models, which calls for further understanding in order to advance the modeling of past and future ozone recovery trends.

Data Availability Statement

The $\mathrm{BASIC_{SG}}$ data set (Alsing & Ball, 2019) has been downloaded from https://data.mendeley.com/datasets/2mgx2xzzpk/3. The CCMI-1 and CCMI-2022 data used in this study are stored at the Centre for Environmental Data Analysis (CEDA) and have been obtained through the British Atmospheric Data Centre (BADC) archive. CCMI-1 data have been downloaded from https://data.ceda.ac.uk/badc/wcrp-ccmi/data/CCMI-1/output and CCMI-2022 from https://data.ceda.ac.uk/badc/ccmi/data/post-cmip6/ccmi-2022. Data from the ERA-5 reanalysis (Hersbach et al., 2020) are available in the Climate Data Store (Copernicus Climate Change Service, Climate Data Store, 2023) at the following link: https://cds.climate.copernicus.eu/datasets/reanalysis-era5-pressure-levels?tab=download. Data of the TEM residual circulation for ERA-5 are available at https://doi.org/10.5281/zenodo.7081436 (Serva, 2022).

Acknowledgments
Samuel Benito-Barca acknowledges the FPU program from the Ministry of Universities (Grant FPU19/01481). Natalia Calvo and Marta Abalos were supported by the Spanish Ministry of Science, Innovation and Universities through the RecO3very project (ref: PID2021-124772OB-I00). Shingo Watanabe was supported by the MEXT program for the advanced studies of climate change projection (SENTAN) Grant JPMXD0722681344. The MIROC-ES2H simulations were conducted using the Earth Simulator at the Japan Agency for Marine-Earth Science and Technology (JAMSTEC). Hideharu Akiyoshi acknowledges KAKENHI (JP24K00700 and JP24H00751) of the Ministry of Education, Culture, Sports, Science, and Technology, Japan, and NEC SX-AURORA computers at the CGER, NIES.

References

Abalos, M., Calvo, N., Benito-Barca, S., Garny, H., Hardiman, S. C., Lin, P., et al. (2021). The Brewer-Dobson circulation in CMIP6. *Atmospheric Chemistry and Physics*, *21*(17), 13571–13591. https://doi.org/10.5194/acp-21-13571-2021

Abalos, M., Randel, W. J., Kinnison, D. E., & Serrano, E. (2013). Quantifying tracer transport in the tropical lower stratosphere using WACCM. *Atmospheric Chemistry and Physics*, *13*(21), 10591–10607. https://doi.org/10.5194/acp-13-10591-2013

Akiyoshi, H., Kadowaki, M., Yamashita, Y., & Nagatomo, T. (2023). Dependence of column ozone on future ODSs and GHGs in the variability of 500-ensemble members. *Scientific Reports*, *13*(1), 1–12. https://doi.org/10.1038/s41598-023-27635-y

Alsing, J., & Ball, W. (2019). BASIC composite ozone time-series data [Dataset]. *Mendeley Data*, *V3*. https://doi.org/10.17632/2mgx2xzzpk.3

Archibald, A. T., M O'Connor, F., Luke Abraham, N., Archer-Nicholls, S., P Chipperfield, M., Dalvi, M., et al. (2020). Description and evaluation of the UKCA stratosphere-troposphere chemistry scheme (StratTrop vn 1.0) implemented in UKESM1. *Geoscientific Model Development*, *13*(3), 1223–1266. https://doi.org/10.5194/gmd-13-1223-2020

Ball, W. T., Alsing, J., Mortlock, D. J., Rozanov, E. V., Tummon, F., & Haigh, J. D. (2017). Reconciling differences in stratospheric ozone composites. *Atmospheric Chemistry and Physics*, *17*(20), 12269–12302. https://doi.org/10.5194/acp-17-12269-2017

Ball, W. T., Alsing, J., Mortlock, D. J., Staehelin, J., Haigh, J. D., Peter, T., et al. (2018). Evidence for a continuous decline in lower stratospheric ozone offsetting ozone layer recovery. *Atmospheric Chemistry and Physics*, *18*(2), 1379–1394. https://doi.org/10.5194/acp-18-1379-2018

Ball, W. T., Alsing, J., Staehelin, J., Davis, S. M., Froidevaux, L., & Peter, T. (2019). Stratospheric ozone trends for 1985–2018: Sensitivity to recent large variability. *Atmospheric Chemistry and Physics*, *19*(19), 12731–12748. https://doi.org/10.5194/acp-19-12731-2019

Ball, W. T., Chiodo, G., Abalos, M., Alsing, J., & Stenke, A. (2020). Inconsistencies between chemistry-climate models and observed lower stratospheric ozone trends since 1998. *Atmospheric Chemistry and Physics*, *20*(16), 9737–9752. https://doi.org/10.5194/acp-20-9737-2020

Benito-Barca, S., Calvo, N., & Abalos, M. (2022). Driving mechanisms for the El Niño-Southern Oscillation impact on stratospheric ozone. *Atmospheric Chemistry and Physics*, *22*(24), 15729–15745. https://doi.org/10.5194/acp-22-15729-2022

Birner, T., & Bönisch, H. (2011). Residual circulation trajectories and transit times into the extratropical lowermost stratosphere. *Atmospheric Chemistry and Physics*, *11*(2), 817–827. https://doi.org/10.5194/acp-11-817-2011

Bognar, K., Tegtmeier, S., Bourassa, A., Roth, C., Warnock, T., Zawada, D., & Degenstein, D. (2022). Stratospheric ozone trends for 1984–2021 in the SAGE II-OSIRIS-SAGE III/ISS composite dataset. *Atmospheric Chemistry and Physics*, *22*(14), 9553–9569. https://doi.org/10.5194/acp-22-9553-2022

Brasseur, G., & Hitchman, M. H. (1988). Stratospheric response to trace gas perturbations: Changes in ozone and temperature distributions. *Science*, *240*(4852), 634–637. https://doi.org/10.1126/science.240.4852.634

Butchart, N. (2014). The Brewer-Dobson circulation. *Reviews of Geophysics*, *52*(2), 157–184. https://doi.org/10.1002/2013RG000448

Calvo, N., Garcia, R. R., Randel, W. J., & Marsh, D. R. (2010). Dynamical mechanism for the increase in tropical upwelling in the lowermost tropical stratosphere during warm ENSO events. *Journal of the Atmospheric Sciences*, *67*(7), 2331–2340. https://doi.org/10.1175/2010JAS3433.1

Carpenter, L. J., Daniel, J. S., Fleming, E. L., Hanaoka, T., Hu, J., Ravishankara, A. R., et al. (2018). Scenarios and information for Policymakers. In *Scientific assessment of ozone depletion: 2018*. World Meteorological Organization.

Chipperfield, M. P., Bekki, S., Dhomse, S., Harris, N. R. P., Hassler, B., Hossaini, R., et al. (2017). Detecting recovery of the stratospheric ozone layer. *Nature*, *549*(7671), 211–218. https://doi.org/10.1038/nature23681

Chipperfield, M. P., Dhomse, S., Hossaini, R., Feng, W., Santee, M. L., Weber, M., et al. (2018). On the cause of recent variations in lower stratospheric ozone. *Geophysical Research Letters*, *45*(11), 5718–5726. https://doi.org/10.1029/2018GL078071

Copernicus Climate Change Service, Climate Data Store. (2023). ERA5 hourly data on pressure levels from 1940 to present [Dataset]. *Copernicus Climate Change Service (C3S) Climate Data Store (CDS)*. https://doi.org/10.24381/cds.bd0915c6

Cussac, M., Marécal, V., Thouret, V., Josse, B., & Sauvage, B. (2020). The impact of biomass burning on upper tropospheric carbon monoxide: A study using MOCAGE global model and IAGOS airborne data. *Atmospheric Chemistry and Physics*, *20*(15), 9393–9417. https://doi.org/10.5194/acp-20-9393-2020

Davis, S. M., Rosenlof, K. H., Hassler, B., Hurst, D. F., Read, W. G., Vömel, H., et al. (2016). The Stratospheric Water and Ozone Satellite Homogenized (SWOOSH) database: A long-term database for climate studies. *Earth System Science Data*, *8*(2), 461–490. https://doi.org/10.5194/essd-8-461-2016

Dennison, F., & Woodhouse, M. T. (2023). ACCESS-CM2-Chem: Evaluation of southern hemisphere ozone and its effect on the southern Annular mode. *Journal of Southern Hemisphere Earth Systems Science*, *73*(1), 17–29. https://doi.org/10.1071/es22015

Dhomse, S. S., Kinnison, D., Chipperfield, M. P., Salawitch, R. J., Cionni, I., Hegglin, M. I., et al. (2018). Estimates of ozone return dates from Chemistry-Climate Model Initiative simulations. *Atmospheric Chemistry and Physics*, *18*(11), 8409–8438. https://doi.org/10.5194/acp-18-8409-2018

Diallo, M., Konopka, P., Santee, M. L., Müller, R., Tao, M., Walker, K. A., et al. (2019). Structural changes in the shallow and transition branch of the Brewer-Dobson circulation induced by El Niño. *Atmospheric Chemistry and Physics*, *19*(1), 425–446. https://doi.org/10.5194/acp-19-425-2019

Dietmüller, S., Garny, H., Eichinger, R., & T. Ball, W. (2021). Analysis of recent lower-stratospheric ozone trends in chemistry climate models. *Atmospheric Chemistry and Physics*, *21*(9), 6811–6837. https://doi.org/10.5194/acp-21-6811-2021

Dietmüller, S., Garny, H., Plöger, F., Jöckel, P., & Cai, D. (2017). Effects of mixing on resolved and unresolved scales on stratospheric age of air. *Atmospheric Chemistry and Physics*, *17*(12), 7703–7719. https://doi.org/10.5194/acp-17-7703-2017

Froidevaux, L., Anderson, J., Wang, H. J., Fuller, R. A., Schwartz, M. J., Santee, M. L., et al. (2015). Global OZone Chemistry and Related Trace gas Data Records for the Stratosphere (GOZCARDS): Methodology and sample results with a focus on HCl, H_2O, and O_3. *Atmospheric Chemistry and Physics*, *15*(18), 10471–10507. https://doi.org/10.5194/acp-15-10471-2015

Froidevaux, L., Kinnison, D. E., Wang, R., Anderson, J., & Fuller, R. A. (2019). Evaluation of CESM1 (WACCM) free-running and specified dynamics atmospheric composition simulations using global multispecies satellite data records. *Atmospheric Chemistry and Physics*, *19*(7), 4783–4821. https://doi.org/10.5194/acp-19-4783-2019

Garcia, R. R., & Solomon, S. (1983). A numerical model of the zonally averaged dynamical and chemical structure of the middle atmosphere. *Journal of Geophysical Research*, *88*(C2), 1379–1400. https://doi.org/10.1029/JC088iC02p01379

Garny, H., Birner, T., Bönisch, H., & Bunzel, F. (2014). The effects of mixing on age of air. *Journal of Geophysical Research: Atmospheres*, *119*(12), 7015–7034. https://doi.org/10.1002/2013JD021417

Gaudel, A., Cooper, O. R., Chang, K. L., Bourgeois, I., Ziemke, J. R., Strode, S. A., et al. (2020). Aircraft observations since the 1990s reveal increases of tropospheric ozone at multiple locations across the Northern Hemisphere. *Science Advances*, *6*(34), 1–11. https://doi.org/10.1126/sciadv.aba8272

Gettelman, A., Mills, M. J., Kinnison, D. E., Garcia, R. R., Smith, A. K., Marsh, D. R., et al. (2019). The Whole Atmosphere Community Climate Model Version 6 (WACCM6). *Journal of Geophysical Research: Atmospheres*, *124*(23), 12380–12403. https://doi.org/10.1029/2019JD030943

Godin-Beekmann, S., Azouz, N., Sofieva, V. F., Hubert, D., Petropavlovskikh, I., Effertz, P., et al. (2022). Updated trends of the stratospheric ozone vertical distribution in the 60°S–60°N latitude range based on the LOTUS regression model. *Atmospheric Chemistry and Physics*, *22*(17), 11657–11673. https://doi.org/10.5194/acp-22-11657-2022

Hersbach, H., Bell, B., Berrisford, P., Hirahara, S., Horányi, A., Muñoz-Sabater, J., et al. (2020). The ERA5 global reanalysis. *Quarterly Journal of the Royal Meteorological Society*, *146*(730), 1999–2049. https://doi.org/10.1002/qj.3803

Jöckel, P., Tost, H., Pozzer, A., Kunze, M., Kirner, O., Brenninkmeijer, C. A. M., et al. (2016). Earth System Chemistry Integrated Modelling (ESCiMo) with the Modular Earth Submodel System (MESSy) version 2.51. *Geoscientific Model Development*, *9*(3), 1153–1200. https://doi.org/10.5194/gmd-9-1153-2016

Jonsson, A. I., de Grandpré, J., Fomichev, V. I., McConnell, J. C., & Beagley, S. R. (2004). Doubled CO_2-induced cooling in the middle atmosphere: Photochemical analysis of the ozone radiative feedback. *Journal of Geophysical Research D: Atmosphere*, *109*(24), 1–18. https://doi.org/10.1029/2004JD005093

Josse, B., Simon, P., & Peuch, V.-H. (2004). Radon global simulations with the multiscale chemistry and transport model MOCAGE. *Tellus B: Chemical and Physical Meteorology*, *56*(4), 339. https://doi.org/10.3402/tellusb.v56i4.16448

Kawamiya, M., Hajima, T., Tachiiri, K., Watanabe, S., & Yokohata, T. (2020). Two decades of Earth system modeling with an emphasis on Model for Interdisciplinary Research on Climate (MIROC). *Progress in Earth and Planetary Science*, *7*(1), 64. https://doi.org/10.1186/s40645-020-00369-5

Keeble, J., Hassler, B., Banerjee, A., Checa-Garcia, R., Chiodo, G., Davis, S., et al. (2021). Evaluating stratospheric ozone and water Vapour changes in CMIP6 models from 1850 to 2100. *Atmospheric Chemistry and Physics*, *21*(6), 5015–5061. https://doi.org/10.5194/acp-21-5015-2021

Liu, J., Strode, S. A., Liang, Q., Oman, L. D., Colarco, P. R., Fleming, E. L., et al. (2022). Change in tropospheric ozone in the recent decades and its contribution to global total ozone. *Journal of Geophysical Research: Atmospheres*, *127*(22). https://doi.org/10.1029/2022JD037170

Marchand, M., Keckhut, P., Lefebvre, S., Claud, C., Cugnet, D., Hauchecorne, A., et al. (2012). Dynamical amplification of the stratospheric solar response simulated with the Chemistry-Climate Model LMDz-Reprobus. *Journal of Atmospheric and Solar-Terrestrial Physics*, *75*(76), 147–160. https://doi.org/10.1016/j.jastp.2011.11.008

Matthes, K., Funke, B., Andersson, M. E., Barnard, L., Beer, J., Charbonneau, P., et al. (2017). Solar forcing for CMIP6 (v3.2). *Geoscientific Model Development*, *10*(6), 2247–2302. https://doi.org/10.5194/gmd-10-2247-2017

Meinshausen, M., Nicholls, Z. R. J., Lewis, J., Gidden, M. J., Vogel, E., Freund, M., et al. (2020). The shared Socio-Economic Pathway (SSP) greenhouse gas concentrations and their extensions to 2500. *Geoscientific Model Development*, *13*(8), 3571–3605. https://doi.org/10.5194/gmd-13-3571-2020

Meinshausen, M., Vogel, E., Nauels, A., Lorbacher, K., Meinshausen, N., Etheridge, D. M., et al. (2017). Historical greenhouse gas concentrations for Climate Modelling (CMIP6). *Geoscientific Model Development*, *10*(5), 2057–2116. https://doi.org/10.5194/gmd-10-2057-2017

Morgenstern, O., Braesicke, P., O'Connor, F. M., Bushell, A. C., Johnson, C. E., Osprey, S. M., & Pyle, J. A. (2009). Evaluation of the new UKCA climate-composition model-Part 1: The stratosphere. *Geoscientific Model Development*, *2*(1), 43–57. https://doi.org/10.5194/gmd-2-43-2009

Morgenstern, O., Hegglin, M., Rozanov, E., O'Connor, F., Luke Abraham, N., Akiyoshi, H., et al. (2017). Review of the global models used within phase 1 of the Chemistry-Climate Model Initiative (CCMI). *Geoscientific Model Development*, *10*(2), 639–671. https://doi.org/10.5194/gmd-10-639-2017

Newman, P. A., Daniel, J. S., Waugh, D. W., & Nash, E. R. (2007). A new formulation of Equivalent Effective Stratospheric Chlorine (EESC). *Atmospheric Chemistry and Physics*, *7*(17), 4537–4552. https://doi.org/10.5194/acp-7-4537-2007

Oman, L. D., Douglass, A. R., Ziemke, J. R., Rodriguez, J. M., Waugh, D. W., & Nielsen, J. E. (2013). The ozone response to Enso in aura satellite measurements and a chemistry-climate simulation. *Journal of Geophysical Research: Atmospheres*, *118*(2), 965–976. https://doi.org/10.1029/2012JD018546

Oman, L. D., Plummer, D. A., Waugh, D. W., Austin, J., Scinocca, J. F., Douglass, A. R., et al. (2010). Multimodel assessment of the factors driving stratospheric ozone evolution over the 21st century. *Journal of Geophysical Research*, *115*(24), 1–21. https://doi.org/10.1029/2010JD014362

O'Neill, B. C., Tebaldi, C., Van Vuuren, D. P., Eyring, V., Friedlingstein, P., Hurtt, G., et al. (2016). The Scenario model Intercomparison project (ScenarioMIP) for CMIP6. *Geoscientific Model Development*, *9*(9), 3461–3482. https://doi.org/10.5194/gmd-9-3461-2016

Orbe, C., Wargan, K., Pawson, S., & Oman, L. D. (2020). Mechanisms linked to recent ozone decreases in the northern hemisphere lower stratosphere. *Journal of Geophysical Research: Atmospheres*, *125*(9), 1–23. https://doi.org/10.1029/2019JD031631

Pazmiño, A., Godin-beekmann, S., Hauchecorne, A., Claud, C., Khaykin, S., Goutail, F., et al. (2018). Multiple symptoms of total ozone recovery inside the Antarctic vortex during austral spring (pp. 7557–7572).

Petropavlovskikh, I., Hubert, D., Damadeo, R., Hassler, B., & Sofieva, V. (2019). SPARC/IO3C/GAW report on long-term ozone trends and uncertainties in the stratosphere. *Sparc/Io3C/Gaw*, *9*.

Plumb, R. A. (2002). Large-scale stratospheric transport processes. *Journal of the Meteorological Society of Japan. Ser. II*, *80*(4B), 793–809. https://doi.org/10.2151/jmsj.80.793

Plummer, D., Nagashima, T., Tilmes, S., Archibald, A., Chiodo, G., Fadnavis, S., et al. (2021). CCMI-2022: A new set of Chemistry-Climate Model Initiative (CCMI) community simulations to update the assessment of models and support upcoming ozone assessment activities. *SPARC Newsletter*, *57*, 22–30.

Portmann, R. W., & Solomon, S. (2007). Indirect radiative forcing of the ozone layer during the 21st century. *Geophysical Research Letters*, *34*(2), 1–5. https://doi.org/10.1029/2006GL028252

Randel, W. J., & Wu, F. (2007). A stratospheric ozone profile data set for 1979–2005: Variability, trends, and comparisons with column ozone data. *Journal of Geophysical Research*, *112*(6), 1–12. https://doi.org/10.1029/2006JD007339

Rayner, N. A., Parker, D. E., Horton, E. B., Folland, C. K., Alexander, L. V., Rowell, D. P., et al. (2003). Global analyses of sea surface temperature, sea ice, and night marine air temperature since the late nineteenth century. *Journal of Geophysical Research*, *108*(14). https://doi.org/10.1029/2002jd002670

Scinocca, J. F., McFarlane, N. A., Lazare, M., Li, J., & Plummer, D. (2008). Technical note: The CCCma third generation AGCM and its extension into the middle atmosphere. *Atmospheric Chemistry and Physics*, *8*(23), 7055–7074. https://doi.org/10.5194/acp-8-7055-2008

Sellar, A. A., Jones, C. G., Mulcahy, J. P., Tang, Y., Yool, A., Wiltshire, A., et al. (2019). UKESM1: Description and evaluation of the U.K. Earth system model. *Journal of Advances in Modeling Earth Systems*, *11*(12), 4513–4558. https://doi.org/10.1029/2019MS001739

Serva, F. (2022). Transformed Eulerian mean data from the ERA5 reanalysis (daily means) [Dataset]. *Zenodo*. https://doi.org/10.5281/zenodo.7081436

Solomon, S., Ivy, D. J., Kinnison, D., Mills, M. J., Neely, R. R., & Schmidt, A. (2016). Emergence of healing in the Antarctic ozone layer. *Science*, *353*(6296), 269–274. https://doi.org/10.1126/science.aae0061

Steinbrecht, W., Froidevaux, L., Fuller, R., Wang, R., Anderson, J., Roth, C., et al. (2017). An update on ozone profile trends for the period 2000 to 2016. *Atmospheric Chemistry and Physics*, *17*(17), 10675–10690. https://doi.org/10.5194/acp-17-10675-2017

Stone, K. A., Solomon, S., & Kinnison, D. E. (2018). On the identification of ozone recovery. *Geophysical Research Letters*, *45*(10), 5158–5165. https://doi.org/10.1029/2018GL077955

Sukhodolov, T., Egorova, T., Stenke, A., Ball, W. T., Brodowsky, C., Chiodo, G., et al. (2021). Atmosphere-ocean-aerosol-chemistry-climate model SOCOLv4.0: Description and evaluation. *Geoscientific Model Development*, *14*(9), 5525–5560. https://doi.org/10.5194/gmd-14-5525-2021

Tatebe, H., Ogura, T., Nitta, T., Komuro, Y., Ogochi, K., Takemura, T., et al. (2019). Description and basic evaluation of simulated mean state, internal variability, and climate sensitivity in MIROC6. *Geoscientific Model Development*, *12*(7), 2727–2765. https://doi.org/10.5194/gmd-12-2727-2019

Villamayor, J., Iglesias-Suarez, F., Cuevas, C. A., Fernandez, R. P., Li, Q., Abalos, M., et al. (2023). Very short-lived halogens amplify ozone depletion trends in the tropical lower stratosphere. *Nature Climate Change*, *13*(6), 554–560. https://doi.org/10.1038/s41558-023-01671-y

Wallace, J. M., Panetta, R. L., & Estberg, J. (1993). Representation of the equatorial stratospheric quasi-biennial oscillation in EOF phase space. *Journal of the Atmospheric Sciences*, *50*(12), 1751–1762. https://doi.org/10.1175/1520-0469(1993)050<1751:ROTESQ>2.0.CO;2

Wang, W., Hong, J., Shangguan, M., Wang, H., Jiang, W., & Zhao, S. (2022). Zonally asymmetric influences of the quasi-biennial oscillation on stratospheric ozone. *Atmospheric Chemistry and Physics*, *22*(20), 13695–13711. https://doi.org/10.5194/acp-22-13695-2022

Wargan, K., Orbe, C., Pawson, S., Ziemke, J. R., Oman, L. D., Olsen, M. A., et al. (2018). Recent decline in extratropical lower stratospheric ozone attributed to circulation changes. *Geophysical Research Letters*, *45*(10), 5166–5176. https://doi.org/10.1029/2018GL077406

Waugh, D. W., & Hall, T. M. (2002). Age of stratospheric air: Theory, observations, and models. *Reviews of Geophysics*, *40*(4). https://doi.org/10.1029/2000RG000101

Weber, M., Arosio, C., Coldewey-Egbers, M., Fioletov, V. E., Frith, S. M., Wild, J. D., et al. (2022). Global total ozone recovery trends attributed to Ozone-Depleting Substance (ODS) changes derived from five merged ozone datasets. *Atmospheric Chemistry and Physics*, *22*(10), 6843–6859. https://doi.org/10.5194/acp-22-6843-2022

WMO. (2022). *Scientific assessment of ozone depletion: Global ozone research and monitoring project—GAW report no. 278*. World Meteorological Organization.

Xie, F., Li, J., Tian, W., Feng, J., & Huo, Y. (2012). Signals of El Niño Modoki in the tropical tropopause layer and stratosphere. *Atmospheric Chemistry and Physics*, *12*(11), 5259–5273. https://doi.org/10.5194/acp-12-5259-2012

Xie, F., Zhang, J., Li, X., Li, J., Wang, T., & Xu, M. (2020). Independent and joint influences of eastern Pacific El Niño–southern oscillation and quasi-biennial oscillation on Northern Hemispheric stratospheric ozone. *International Journal of Climatology*, *40*(12), 5289–5307. https://doi.org/10.1002/joc.6519

Zeng, G., Querel, R., Shiona, H., Poyraz, D., Van Malderen, R., Geddes, A., et al. (2024). Analysis of a newly homogenised ozonesonde dataset from Lauder, New Zealand. *Atmospheric Chemistry and Physics*, *24*(10), 6413–6432. https://doi.org/10.5194/acp-24-6413-2024

Zhang, Y., West, J. J., Emmons, L. K., Flemming, J., Jonson, J. E., Lund, M. T., et al. (2021). Contributions of world regions to the global tropospheric ozone Burden change from 1980 to 2010. *Geophysical Research Letters*, *48*(1), 1–12. https://doi.org/10.1029/2020GL089184

Ziemke, J. R., Oman, L. D., Strode, S. A., Douglass, A. R., Olsen, M. A., McPeters, R. D., et al. (2019). Trends in global tropospheric ozone inferred from a composite record of TOMS/OMI/MLS/OMPS satellite measurements and the MERRA-2 GMI simulation. *Atmospheric Chemistry and Physics*, *19*(5), 3257–3269. https://doi.org/10.5194/acp-19-3257-2019